THE JOURNAL OF PHYSICAL CHEMISTRY C

ARTICLE

pubs.acs.org/JPCC

Synthesis and Photoluminescence Properties of a Novel Red-Emitting $Na_2Y_2Ti_3O_{10}:Eu^{3+},Sm^{3+}$ Phosphor for White-Light-Emitting Diodes

Dongseok Kang, Hyoung Sun Yoo, Sang Hoon Jung, Hyunki Kim, and Duk Young Jeon*

Department of Materials Science and Engineering, Korea Advanced Institute of Science and Technology, 335 Gwahangno, Yuseong-gu, Daejeon 305-701, Republic of Korea

Supporting Information

ABSTRACT: A novel red-emitting $Na_2Y_2Ti_3O_{10}:Eu^{3+},Sm^{3+}$ phosphor was synthesized for the first time, and its photoluminescence (PL) properties were investigated for application to white-light-emitting diodes (W-LEDs). The $Na_2Y_1Eu_1Ti_3O_{10}$ phosphor showed a 3-fold higher PL intensity compared to that of a commercial red-emitting $Y_2O_2S:Eu^{3+}$ phosphor under 396 nm irradiation. Sm^{3+} ions were introduced as a sensitizer, and they increased the PL intensity by up to 35% under 410 nm irradiation. The effects of introducing the sensitizer were investigated by measuring the quantum efficiencies and the time-resolved PL decay curves. The $Na_2Y_1Eu_1Ti_3O_{10}$ phosphor exhibited remarkable resistance to thermal quenching, and a W-LED comprising the phosphor showed bright white emission with a color rendering index (R_a) of 83, a color temperature of 5556 K, and Commission Internationale de I'Eclairage (CIE) color coordinates of (0.3306, 0.3754).

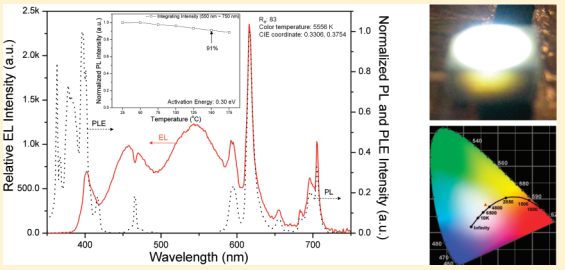

1. INTRODUCTION

Demand for white-light-emitting diodes (W-LEDs) as a next-generation light source is high due to the long lifetimes, high energy efficiency, and environmental friendliness of LEDs. Conventional methods for generating white light using LEDs involve blending light from a blue LED chip with appropriate quantities of a yellow-emitting phosphor, such as cerium-doped yttrium aluminum garnet (YAG:Ce^{3+}), on top of the blue LED chip.[1−3] However, this approach causes several serious problems, such as thermal quenching, a low color rendering index (CRI), and a narrow visible range. Efforts to improve the CRI have included adding red-emitting components, such as red-emitting quantum dots or nitride phosphors.[4−8] The practical utility of these combination chips is restricted. Red-emitting quantum dots, such as CdSe, are toxic, and nitride phosphors have the drawback of a relatively high manufacturing expense due to the severe synthesis conditions and high patent licensing costs.

An alternative approach involves the manufacture of near-UV LED chips by blending red-, green-, and blue-emitting phosphors together on top of an LED chip to assemble W-LEDs.[9] The external quantum efficiency of InGaN LEDs reaches a maximum at 400 nm, and the current density drops off at this point. "Droop" is, therefore, absent from these InGaN-based UV LEDs.[10,11] Moreover, the fabrication of white LEDs using this method can yield a CRI of $R_a \geq 80$, and the emission color properties, such as color temperature, may be easily controlled. Nevertheless, the blending of red-, green-, and blue-emitting phosphors together is impractical for near-UV LED chips due to the poor efficiency caused by a large Stokes shift between excitation and emission in the UV-excitable phosphor. Therefore, it is important to develop efficient novel phosphors, particularly red-emitting phosphors, that can be excited efficiently under near-UV irradiation.

Phosphors containing Eu^{3+} ions as activators can emit red light. Their excitation bands usually consist of host lattice excitation bands, charge-transfer bands, and direct excitation bands.[12] An oxide host lattice produces direct excitation bands in the near-UV region, although the host lattice excitation bands and charge-transfer bands do not generally reach the near-UV region. However, direct excitation bands have a low absorption cross section because the direct excitation of Eu^{3+} involves a forbidden transition. Phosphors with layered structures occasionally show interestingly strong direct excitation bands.[13−15] At the same time, the critical concentration of the activator ions can be much higher than that observed in conventional inorganic phosphors.[16−18] Energy migration among activators is restricted to a two-dimensional activator layer.[18] Therefore, layered phosphor structures, in which Eu^{3+} ions are doped at a high concentration in the two-dimensional host lattice, present a promising way to seek novel red-emitting phosphors that are efficiently excited under near-UV irradiation.

In this study, we have tested $Na_2Y_2Ti_3O_{10}$ as a host lattice. This material belongs to the $Na_2Ln_2Ti_3O_{10}$ (Ln = lanthanide ions) group containing triple perovskite layers. Such materials have been studied for use as photocatalysts, ion-exchangeable materials, and phosphors.[18−21] $Na_2Y_2Ti_3O_{10}$ itself is a novel

Received: March 24, 2011
Revised: October 9, 2011
Published: October 10, 2011

composition. The photoluminescence (PL) properties of the $Na_2Y_2Ti_3O_{10}$:Eu^{3+} phosphor and the effects of codoping with the Sm^{3+} ion on the PL properties were investigated in detail. Finally, the generation of red or white light and the fabrication of W-LEDs by incorporating green-emitting $Sr_{1.95}Eu_{0.05}Si_2O_2N_2$ and blue-emitting $BaMgAl_{12}O_{19}$:Eu^{2+} phosphors will be discussed along with their luminescence properties.

2. EXPERIMENTAL SECTION

The $Na_2Y_2Ti_3O_{10}$:Eu^{3+},Sm^{3+} phosphor samples were prepared by solid-state reaction methods. Na_2CO_3 (Aldrich, 99.995%), Y_2O_3 (Kojundo, 99.9%), TiO_2 (Kojundo, 99.9%), Eu_2O_3 (GCM, 99.99%), and Sm_2O_3 (Aldrich, 99.999%) were used as raw materials to prepare the phosphor samples. An excess Na_2CO_3 of up to 75 mol % was used. The samples were sintered at temperatures between 1150 and 1350 °C for 3 h in ambient air.

The crystalline phases of the phosphor were analyzed using a Rigaku D/max-RB X-ray diffractometer (XRD) with Cu Kα (λ = 1.542 Å) radiation operated at 40 kV and 100 mA. The scan rate was 2°/min and the measurement range was between 5° and 65°. PL and PL excitation (PLE) spectra were recorded using a DARSA PRO 5100 PL System (PSI, Korea) or F-7000 fluorescence spectrophotometer (Hitachi, Japan). The PLE spectra recorded by either instrument were corrected using sodium salicylate and Rhodamine B, respectively. The time-resolved PL decay curves were recorded using a F-7000 fluorescence spectrophotometer (Hitachi, Japan). To obtain the internal quantum efficiency (IQE), external quantum efficiency (EQE), and absorptance of the phosphor samples, an integrating sphere was included in the F-7000 fluorescence spectrophotometer (Hitachi, Japan). The quantum efficiencies were corrected by subtracting a proportion of the emission, which resulted from re-excitation due to the reflected excitation source within the integrating sphere (Supporting Information).[22]

To fabricate W-LEDs, near-UV LEDs (λ_{max} = 400 nm) were first fabricated using red-emitting $Na_2Y_1Eu_1Ti_3O_{10}$, green-emitting $Sr_{1.95}Eu_{0.05}Si_2O_2N_2$, and blue-emitting $BaMgAl_{12}O_{19}$:Eu^{2+} phosphors mixed with silicone resin. The as-fabricated LED chips containing the phosphors were subsequently heated at 80 °C for 5 h.[23] The electroluminescence (EL) properties of the as-prepared W-LED chips, such as the EL spectra, CRI, and Commission Internationale de l'Eclairage (CIE) color coordinates, were characterized using a DARSA PRO 5100 PL system (PSI, Korea) under a forward bias current of 20 mA at room temperature, located within an integrating sphere. The temperature dependence of the PL intensity was recorded using a DARSA PRO 5100 PL system (PSI, Korea) as well.

3. RESULTS AND DISCUSSION

3.1. Synthesis. A single phase of the novel $Na_2Y_2Ti_3O_{10}$ host lattice was synthesized in the presence of excess Na_2CO_3 at an optimized sintering temperature. Figure 1a shows the XRD patterns of the $Na_2Y_2Ti_3O_{10}$ host lattice samples prepared in the presence of various amounts of excess Na_2CO_3 along with the $Na_2Eu_2Ti_3O_{10}$ reference pattern (83-0142). All samples were sintered at 1150 °C for 3 h, and the samples contained the $NaYTiO_4$ phase or other unknown impurities, as shown in Figure 1a. As the excess Na_2CO_3 was increased, the XRD intensity of the peaks from the $NaYTiO_4$ phase increased, and the XRD intensity of the unknown phase decreased. A higher Na

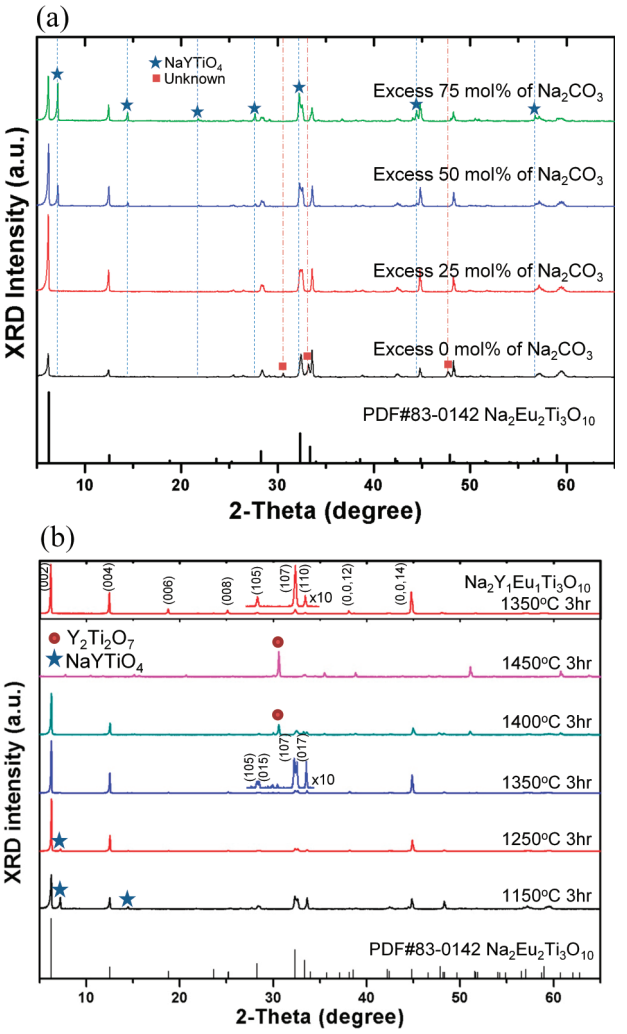

Figure 1. (a) XRD patterns of the $Na_2Y_2Ti_3O_{10}$ host lattice samples for various amounts of excess Na_2CO_3, compared with the $Na_2Eu_2Ti_3O_{10}$ reference pattern (83-0142). All samples were sintered at 1150 °C for 3 h. Filled asterisks and filled squares indicate the $NaYTiO_4$ phase and an unknown impurity phase, respectively. (b) XRD patterns of $Na_2Y_2Ti_3O_{10}$ samples sintered at various sintering temperatures for 3 h, as well as one $Na_2Y_1Eu_1Ti_3O_{10}$ sample, and the $Na_2Eu_2Ti_3O_{10}$ reference pattern (83-0142). Filled asterisks and filled circles indicate $NaYTiO_4$ and $Y_2Ti_2O_7$ impurity phases, respectively.

content formed a Na-rich $NaYTiO_4$ phase (Na/Ti = 1:1) rather than the $Na_2Y_2Ti_3O_{10}$ phase (Na/Ti = 2:3), with a lower Na content. At the same time, the overall XRD intensity tended to increase, suggesting that the crystallinity of the compositions improved. The excess Na_2CO_3 apparently not only acts as a flux material but also compensates for the loss due to sodium evaporation during the sintering process.[14]

The XRD patterns of the $Na_2Y_2Ti_3O_{10}$ host lattice samples prepared at various sintering temperatures are shown in Figure 1b. All samples were sintered with a 50 mol % excess Na_2CO_3. The XRD patterns of the sample sintered at 1350 °C for 3 h resembled the $Na_2Eu_2Ti_3O_{10}$ reference pattern (83-0142). However, slight peak splitting was observed at the (a b c) ($a \neq b$) planes, remarkably at the (105) and (107) planes. This result suggests that the $Na_2Y_2Ti_3O_{10}$ crystal system was orthorhombic, whereas the $Na_2Ln_2Ti_3O_{10}$ (Ln = La, Nd, Sm, Eu, Gd)

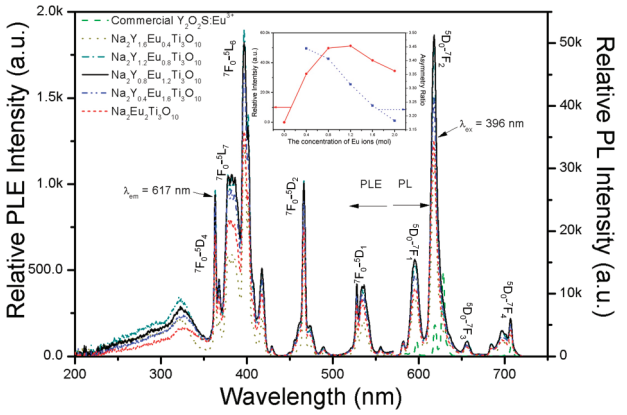

Figure 2. PLE spectra (λ_{em} = 617 nm) and PL spectra (λ_{ex} = 396 nm) of $Na_2Y_{2-x}Eu_xTi_3O_{10}$ phosphor samples prepared for various concentrations of Eu^{3+}, compared to the PL spectrum (λ_{ex} = 396 nm) of a commercial red-emitting $Y_2O_2S:Eu^{3+}$ phosphor. The inset shows the relative PL intensity and asymmetry ratio for each sample.

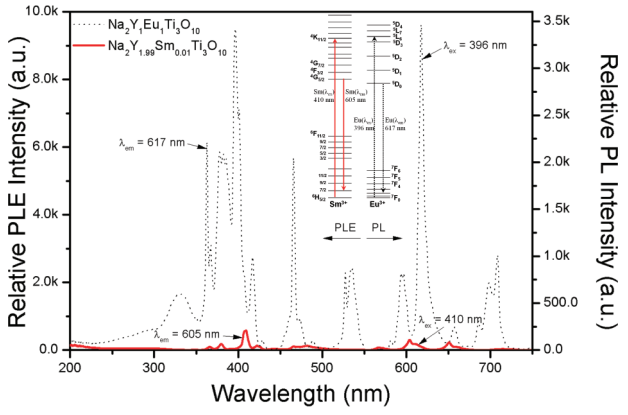

Figure 3. PLE (λ_{em} = 605 nm) and PL (λ_{ex} = 410 nm) spectra of a $Na_2Y_{1.99}Sm_{0.01}Ti_3O_{10}$ phosphor compared to those of a $Na_2Y_1Eu_1Ti_3O_{10}$ phosphor. The inset shows the most intense excitation and emission process within the intra-4f levels of Eu^{3+} and Sm^{3+} ions.

system is known to be tetragonal. Presumably, the small ionic radius of the Y^{3+} ion, compared to the ionic radii of La^{3+}, Nd^{3+}, Sm^{3+}, Eu^{3+}, or Gd^{3+} ions, caused such lattice restructuring. As the sintering temperature increased, the XRD intensity of the peaks due to the Na-rich $NaYTiO_4$ (Na/Ti = 1:1) phase decreased and the XRD intensity of peaks due to the Na-free $Y_2Ti_2O_7$ phase increased. The evaporation of Na ions appeared to accelerate as the sintering temperature increased. Therefore, if the excess Na_2CO_3 concentration was adjusted, optimized conditions, such as the sintering temperature and duration, may be controlled to obtain single-phase $Na_2Y_2Ti_3O_{10}$. The synthesis conditions for the $Na_2Y_{2-x}Eu_xTi_3O_{10}$ phosphor samples were found to be optimal with sintering at 1350 °C for 3 h in the presence of a 50 mol % excess of Na_2CO_3.

3.2. Photoluminescence Properties of $Na_2Y_2Ti_3O_{10}:Eu^{3+}$. Figure 2 shows the PL and PLE spectra of the $Na_2Y_{2-x}Eu_xTi_3O_{10}$ phosphor samples under 396 nm irradiation. The PL spectra of all samples consisted of characteristic sharp lines that originated from the intra-4f transitions of Eu^{3+} ions, as indicated in Figure 2. The peak emission wavelength was monitored at 617 nm, assigned to the $^5D_0$–$^7F_2$ transition observed when Eu^{3+} ions occupied sites with noninversion symmetry.[24,25] The PLE spectra of the $Na_2Y_{2-x}Eu_xTi_3O_{10}$ phosphor samples monitored at 617 nm consisted of broad bands and sharp lines. The major excitation transitions in the samples were intra-4f transitions (sharp lines, 350–600 nm region), and the peak excitation wavelength was observed at 396 nm, assigned to the $^7F_0$–$^5L_6$ transition.[26] This result demonstrates that a $Na_2Y_{2-x}Eu_xTi_3O_{10}$ phosphor is a promising red-emitting component that may be applied to W-LEDs using near-UV LED chips. The inset of Figure 2 presents the relative PL intensities and asymmetry ratios of the $Na_2Y_{2-x}Eu_xTi_3O_{10}$ phosphor samples monitored at 617 nm, for various concentrations of Eu^{3+} ions. The PL intensities of the $Na_2Y_{0.8}Eu_{1.2}Ti_3O_{10}$ or $Na_2Y_{1.2}Eu_{0.8}Ti_3O_{10}$ phosphor samples were about 3 times the intensity of a commercial red-emitting $Y_2O_2S:Eu^{3+}$ phosphor, and the critical concentration of the $Na_2Y_{2-x}Eu_xTi_3O_{10}$ phosphor was determined to be around 50 mol % Eu^{3+} ions. Such an activator concentration is unusually high among typical phosphors. These trends are usually observed when activators are arranged in low-dimensional structures such that excited energy migration among activators is considerably limited.[14,27] The IQE and EQE of the $Na_2Y_1Eu_1Ti_3O_{10}$ phosphor were around 40% and 20%, respectively, under 396 nm irradiation.

As depicted in Figure 1b, substituting 1 mol of Eu^{3+} ions for the Y^{3+} ions produced a tetragonal $Na_2Y_1Eu_1Ti_3O_{10}$ phosphor crystal system, which is higher in symmetry than the orthorhombic structure. The same trend was evident upon examination of the ($^5D_0$–$^7F_2$)/($^5D_0$–$^7F_1$) intensity ratio, the asymmetry ratio, which suggests the degree of distortion, with respect to inversion symmetry, of the local Eu^{3+} ion environments in the lattice.[24,25] The electric dipole transition $^5D_0$–$^7F_2$ (617 nm) is hypersensitive to distortion of the inversion symmetry, whereas the magnetic dipole transition $^5D_0$–$^7F_1$ (595 nm) is insensitive to it. As shown in the inset of Figure 2, the asymmetry ratio decreased as the concentration of Eu^{3+} ions increased, as expected.

3.3. Effects of Codoping Sm^{3+} Ions. Figure 3 shows a comparison of the PLE and PL spectra of the Sm^{3+}-doped $Na_2Y_2Ti_3O_{10}$ phosphor with that of the Eu^{3+}-doped phosphor. Such spectra usually consist of sharp characteristic lines and weak broad bands, as in the Eu^{3+}-doped spectrum. The peak excitation and emission wavelengths were located at 410 nm ($^6H_{5/2}$–$^4K_{11/2}$) and 605 nm ($^4G_{5/2}$–$^6H_{7/2}$), respectively.[28,29]

Energy transfer from Sm^{3+} to Eu^{3+} is nonresonant and phonon-assisted.[12,30,31] The energy transfer is very efficient at room temperature. Not only is the $^4G_{5/2}$ level of Sm^{3+} slightly higher than the $^5D_0$ level of Eu^{3+}, as shown in the inset of Figure 3, but also the energy transfer rate is much faster than the emission rate of Sm^{3+} or Eu^{3+}.[30] The PLE and PL spectra of the $Na_2Y_{1-y}Eu_1Sm_yTi_3O_{10}$ phosphor samples are presented in Figure 4. As the concentration of Sm^{3+} ions increased, the shape of the PL spectra became more uniform. However, the shape of the PLE spectrum changed. In particular, the PLE intensity of the peaks located between 400 and 410 nm (the range of the peak excitation wavelength of $Na_2Y_{2-y}Sm_yTi_3O_{10}$ phosphors) increased slightly up to 0.01 mol of Sm^{3+}, as shown in the inset of Figure 4. In this range, as shown in Table 1, the absorptance of the $Na_2Y_1Eu_1Ti_3O_{10}$ phosphor was found to be only 0.095. However, the phosphor absorptance increased up to 0.17 upon codoping with 0.01 mol of Sm^{3+}, comparable to the absorptance of the $Na_2Y_{1.99}Sm_{0.01}Ti_3O_{10}$ phosphor. As a result, the $Na_2Y_{0.99}Eu_1Sm_{0.01}Ti_3O_{10}$ phosphor displayed a 35% higher

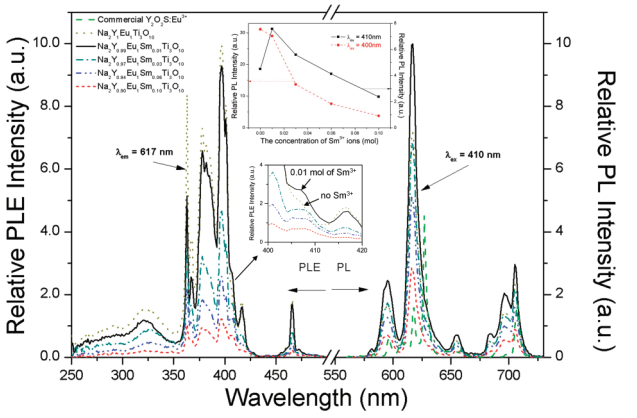

Figure 4. PLE spectra ($\lambda_{em} = 617$ nm) and PL spectra ($\lambda_{ex} = 410$ nm) of $Na_2Y_{1-y}Eu_1Sm_yTi_3O_{10}$ phosphor samples prepared with various concentrations of Sm^{3+}, compared to the PL spectrum ($\lambda_{ex} = 410$ nm) of a commercial red-emitting $Y_2O_2S:Eu^{3+}$ phosphor. The inset shows the relative PL intensity of the Eu^{3+} ion emission ($\lambda_{em} = 617$ nm) as a function of Sm^{3+} concentration.

Table 1. Quantum Efficiency of the Phosphor Samples Measured under 410 nm Irradiation

	$Na_2Y_1Eu_1$-Ti_3O_{10}	$Na_2Y_{0.99}$-$Eu_1Sm_{0.01}Ti_3O_{10}$	$Na_2Y_{1.99}$-$Sm_{0.01}Ti_3O_{10}$
IQE (%)	25	19	6.6
absorptance	0.095	0.17	0.17
EQE (%)	2.4	3.2	1.1

PL intensity and EQE compared to those of the $Na_2Y_1Eu_1$-Ti_3O_{10} phosphor under 410 nm irradiation, even though the former had a lower IQE than the latter. The lower IQE appeared to result from strong cross-relaxation among Sm^{3+} ions.[30] The PL and PLE intensities of the $Na_2Y_{1-y}Eu_1Sm_y$-Ti_3O_{10} phosphor samples containing more than 0.01 mol of Sm^{3+} were quenched by energy migration, as shown in the inset of Figure 4.

The energy-transfer phenomenon and the decreased IQE with codoping of Sm^{3+} were investigated by analyzing the time-resolved PL decay curves for the phosphor samples. These curves may be described approximately using the equation

$$I = I_0 \exp\left(-\frac{\tau}{\tau_0}\right) \quad (1)$$

where τ_0 is the emission decay constant.[12] As the concentration of Sm^{3+} ions increased, the shape of the PL emission decay curves for Eu^{3+} ions apparently shifted from exponential to nonexponential forms, as depicted in Figure 5a. This shift revealed the presence of more than one relaxation process. Additionally, in the presence of the nonresonant energy transfer, the emission decay constant of Sm^{3+} should be shortened.[12] Figure 5b presents the emission decay curve for Sm^{3+}. To exclude Eu^{3+} emission and record only Sm^{3+} emission, the emission peak at 567 nm was monitored. As a result, the contribution of the Eu^{3+} ions to the measured decay curve increased and the decay constant for Sm^{3+} emission decreased. The change in shape of the PLE spectra and the decreased decay constant for Sm^{3+} ion emission

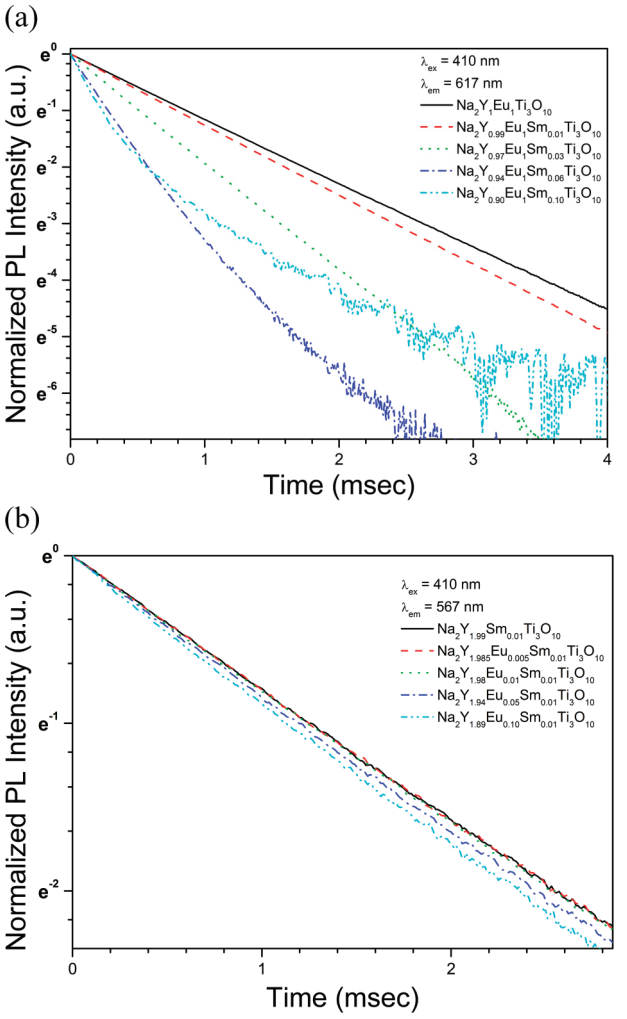

Figure 5. Time-resolved PL decay curves of (a) $Na_2Y_{1-y}Eu_1Sm_yTi_3O_{10}$ phosphor samples with various concentrations of Sm^{3+}, monitored at 617 nm under 410 nm irradiation, and (b) $Na_2Y_{1.99-x}Eu_xSm_{0.01}Ti_3O_{10}$ phosphor samples with various concentrations of Eu^{3+}, monitored at 567 nm under 410 nm irradiation. All curves were calculated by averaging 10 independent recordings.

suggest that the energy absorbed by Sm^{3+} ions was transferred to the Eu^{3+} ions.

Because the shape of the PL spectra remained unchanged, the decrease in τ_0 was regarded as a decrease in IQE (η) related to a $^5D_0 - {}^7F_{0-4}$ transition for Eu^{3+} ions, according to the following equations[32,33]

$$k_{rad} = A_{0-1}\frac{\hbar\omega_{0-1}}{S_{0-1}}\sum_{J=0}^{4}\frac{S_{0-J}}{\hbar\omega_{0-J}} \quad (2)$$

$$k_{exp} = \tau_0^{-1} = k_{rad} + k_{nonrad} \quad (3)$$

$$\eta = \frac{k_{rad}}{k_{rad} + k_{nonrad}} \quad (4)$$

where k_{rad} is the radiative transition rate, k_{nonrad} is the nonradiative transition rate, A_{0-1} is Einstein's coefficient for spontaneous emission between the $^5D_0$ and $^7F_1$ levels, $\hbar\omega$ refers to the energy barrier, and S is the area under the emission curve.

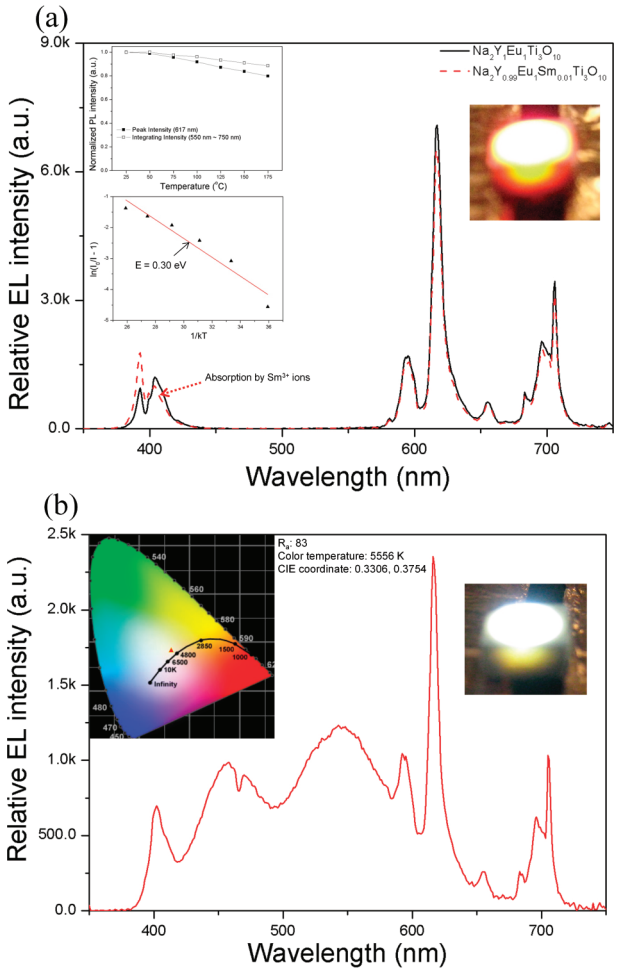

Figure 6. (a) EL spectra of $Na_2Y_1Eu_1Ti_3O_{10}$ and $Na_2Y_{0.99}Eu_1Sm_{0.01}Ti_3O_{10}$ phosphor-based red LEDs under a forward bias current of 20 mA. The inset shows the temperature dependence of the PL intensity, the integrating intensity, and the activation energy for thermal quenching of the $Na_2Y_1Eu_1Ti_3O_{10}$ phosphor. (b) EL spectrum of $Na_2Y_1Eu_1Ti_3O_{10}$, $Sr_{1.95}Eu_{0.05}Si_2O_2N_2$, and $BaMgAl_{12}O_{19}:Eu^{2+}$ phosphor-based W-LEDs under a forward bias current of 20 mA. The inset shows the CIE color coordinate of the EL spectrum.

The above equations may be simplified as follows

$$\eta = \frac{k_{rad}}{k_{rad} + k_{nonrad}} = \frac{k_{rad}}{\tau_0^{-1}} = k_{rad} \times \tau_0 \qquad (5)$$

Here, k_{rad} is determined by the emission spectrum and can be fixed so long as the emission spectrum remains unchanged. Therefore, according to eq 5, IQE (η) for the $Na_2Y_{1-y}Eu_1Sm_yTi_3O_{10}$ phosphors decreased as the Sm^{3+} content increased. This result is identical to that presented in Table 1. Li et al. investigated the relationship between the decay constant and the concentration of Eu^{3+} ions in a phosphor.[34] Their study demonstrated that the decay constant of the phosphor decreased steeply around a critical concentration. By taking Li's study and eq 5 into account, we expect the IQE (η) of the phosphor to decrease steeply around the critical concentration. $Na_2(Y,Eu)_2Ti_3O_{10}$ phosphors with Eu^{3+} concentrations lower than the critical concentration would show an IQE (η) greater than 40% (Supporting Information).

3.4. Thermal Quenching and Fabrication of W-LEDs. Thermal quenching is an important consideration for the application of phosphors in W-LEDs. The inset of Figure 6a shows the temperature dependence of the PL intensity and the integrating intensity of a $Na_2Y_1Eu_1Ti_3O_{10}$ phosphor sample. At 150 °C, the PL intensity and the integrating intensity decreased by only 16% and 9%, respectively, which is remarkable, even in comparison with the properties of the red-emitting nitride phosphor.[35] Such a high resistance to thermal quenching originated from the uncrossed ground and excited states within the intra-4f levels of Eu^{3+}.[36] The temperature dependence of the PL intensity was dominated by multiphonon nonradiative transitions. The highest available vibrational frequency of a Eu^{3+} ion environment and the energy difference of the radiative transition were 910 and 12 000 cm^{-1}, respectively.[12,37−39] To fulfill the condition of multiphonon nonradiative transitions, the ratio of the energy difference to the vibrational frequency should be less than 5 to 1. The increase in the energy migration rate apparently caused thermal quenching. The temperature dependence of the energy migration rate became exponential ($\exp(-\Delta E/kT)$) as the temperature increased. Moreover, if the Eu−Eu distance were smaller than 5 Å, the exponential behavior would become more effective.[12] The distance between Eu^{3+} ion sites within the $Na_2Eu_2Ti_3O_{10}$ phosphor was 3.8−4.3 Å.[18] $Na_2Y_1Eu_1Ti_3O_{10}$ phosphors are expected to feature similar Eu^{3+} distances because the XRD pattern of the $Na_2Y_1Eu_1Ti_3O_{10}$ phosphors resembled that of $Na_2Eu_2Ti_3O_{10}$, as shown in Figure 1b. Therefore, it is possible that the nonradiative transition rate of $Na_2Y_1Eu_1Ti_3O_{10}$ phosphors followed an exponential form, and eq 4 may be modified as follows

$$\frac{I}{I_0} \approx \eta = \frac{k_{rad}}{k_{rad} + k_{nonrad}} = \frac{k_{rad}}{k_{rad} + A\exp\left(-\frac{\Delta E}{kT}\right)} \qquad (6)$$

$$I \approx \frac{I_0}{1 + A'\exp\left(-\frac{\Delta E}{kT}\right)} \qquad (7)$$

where I is the intensity at a given temperature, I_0 is the initial intensity, k is the Boltzmann's constant, T is temperature, and ΔE is the activation energy and can be regarded as a constant because the shape of the emission curve did not change significantly. This equation takes the same form as the Arrhenius equation.[35,40] Consequently, the activation energy of the $Na_2Y_1Eu_1Ti_3O_{10}$ phosphor was 0.30 eV, as shown in the inset of Figure 6a. This value was higher value than that of a red-emitting nitride phosphor.[35]

Figure 6 presents the EL spectra of $Na_2Y_1Eu_1Ti_3O_{10}$ and $Na_2Y_{0.99}Eu_1Sm_{0.01}Ti_3O_{10}$ phosphor-based red LEDs under a forward bias current of 20 mA. Both red LEDs exhibited intense red light under the same conditions. Figure 6a shows noticeable differences in the spectral shapes of the emitted near-UV light. The $Na_2Y_{0.99}Eu_1Sm_{0.01}Ti_3O_{10}$ phosphor-based red LED exhibited a higher absorption in the 410 nm region, as expected.

Figure 6b presents the EL spectrum of a W-LED comprising $Na_2Y_1Eu_1Ti_3O_{10}$, $Sr_{1.95}Eu_{0.05}Si_2O_2N_2$, and $BaMgAl_{12}O_{19}:Eu^{2+}$ phosphors under a forward bias current of 20 mA. The W-LED exhibited intense white light under the same conditions. Reabsorption by the red phosphor, one of the critical problems in multiphosphor-based W-LEDs, was only weakly observed at 465 nm ($^7F_0$−$^5D_2$). In fact, this problem could not be avoided

among red-emitting phosphors with broad band emission, such as Eu^{2+}- or Ce^{3+}-activated phosphors. The R_a of the W-LED was about 83, which is sufficient for use as a lighting device. The color temperature and CIE coordinates of the W-LED were 5556 K and (0.3306, 0.3754), respectively, as shown in the inset of Figure 6b. It was possible to control the performance of the W-LED by adjusting the combination of phosphors.

4. CONCLUSIONS

To develop a novel red-emitting phosphor for near-UV LED-based W-LED applications, a $Na_2Y_2Ti_3O_{10}:Eu^{3+},Sm^{3+}$ phosphor was synthesized for the first time, and its luminescence properties were investigated. Red and white LEDs comprising this novel phosphor were fabricated. The phosphor samples emitted bright red light under near-UV irradiation, and peak excitation and emission wavelengths were observed at 396 and 617 nm, respectively. The $Na_2Y_1Eu_1Ti_3O_{10}$ phosphor emitted at 3 times the intensity of a commercial red-emitting $Y_2O_2S:Eu^{3+}$ phosphor, and its IQE and EQE were 40% and 20%, respectively, under 396 nm irradiation. By codoping with Sm^{3+} ions, the PL intensity increased up to 135% under 410 nm irradiation, even though the IQE decreased. These properties were mechanistically understood by examining the quantum efficiencies and time-resolved PL decay curves. The enhancement in PL intensity due to codoping with Sm^{3+} resulted from the higher absorptance of Sm^{3+} ions, which outweighed the lower IQE of the Sm^{3+} ions. The $Na_2Y_1Eu_1Ti_3O_{10}$ phosphor exhibited a remarkably high resistance to thermal quenching, which did not originate from multiphonon nonradiative transitions. The difference between the highest available vibrational frequency of the Eu^{3+} environment and the energy associated with a radiative transition were not comparable. Most likely, the resistance to thermal quenching originated from an increase in the energy migration rate. The red and W-LEDs comprising the $Na_2Y_1Eu_1Ti_3O_{10}$ phosphor showed bright red and white light. The W-LED showed a color rendering index of 83, which is sufficient for use in lighting devices.

■ ASSOCIATED CONTENT

Supporting Information. Quantum efficiencies (QEs) of $Na_2Y_1Eu_1Ti_3O_{10}$ and $Y_2O_2S:Eu^{3+}$ measured using an F-7000 fluorescence spectrophotometer (Hitachi, Japan) and the quantum efficiency correction method, and decay curves and calculated quantum efficiencies of $Na_2Y_{2-x}Eu_xTi_3O_{10}$ phosphors. This material is available free of charge via the Internet at http://pubs.acs.org.

■ AUTHOR INFORMATION

Corresponding Author

*Fax: +82-42-350-3310. Tel: +82-42-350-3337. E-mail: dyj@kaist.ac.kr.

■ ACKNOWLEDGMENT

This work was supported by the Components & Materials Technology Development program of the Ministry of Knowledge Economy (Grant No. 10036981).

■ REFERENCES

(1) Hoppe, H. A. *Angew. Chem., Int. Ed.* **2009**, *48*, 3572–3582.
(2) Feldmann, C.; Justel, T.; Ronda, C. R.; Schmidt, P. J. *Adv. Funct. Mater.* **2003**, *13*, 511–516.
(3) Ye, S.; Xiao, F.; Pan, Y. X.; Ma, Y. Y.; Zhang, Q. Y. *Mater. Sci. Eng., R* **2010**, *71*, 1–34.
(4) Jang, H. S.; Yang, H.; Kim, S. W.; Han, J. Y.; Lee, S.-G.; Jeon, D. Y. *Adv. Mater.* **2008**, *20*, 2696–2702.
(5) Jang, H. S.; Kwon, B.-H.; Yang, H.; Jeon, D. Y. *Appl. Phys. Lett.* **2009**, *95*, 161901.
(6) Kimura, N.; Sakuma, K.; Hirafune, S.; Asano, K.; Hirosaki, N.; Xie, R.-J. *Appl. Phys. Lett.* **2007**, *90*, 051109.
(7) Kimura, N.; Sakuma, K.; Hirafune, S.; Asano, K.; Liu, R.-S.; Hu, S.-F. *Appl. Phys. Lett.* **2007**, *90*, 123503.
(8) Xie, R.-J.; Hirosaki, N.; Suehiro, T.; Xu, F.-F.; Mitomo, M. *Chem. Mater.* **2006**, *18*, 5578–5583.
(9) Sato, Y.; Takahashi, N.; Sato, S. *Jpn. J. Appl. Phys.* **1996**, *35*, L838–L839.
(10) Krames, M. R.; Shchekin, O. B.; Mueller-Mach, R.; Mueller, G. O.; Zhou, L.; Harbers, G.; Craford, M. G. *J. Disp. Technol.* **2007**, *3*, 160–175.
(11) Yang, Y.; Cao, X. A.; Yan, C. *IEEE Trans. Electron Devices* **2008**, *55*, 1771–1775.
(12) Blasse, G.; Grabmaier, B. C. *Luminescent Materials*; Springer-Verlag: Berlin, 1994.
(13) Vaidyanathan, S.; Jeon, D. Y. *Int. J. Appl. Ceram. Technol.* **2009**, *6*, 453–458.
(14) Toda, K.; Honma, T.; Sato, M. *J. Lumin.* **1997**, *71*, 71–75.
(15) Wanga, Z.; Liang, H.; Wang, Q.; Luo, L.; Gong, M. *Mater. Sci. Eng., B* **2009**, *164*, 120–123.
(16) De Vries, A. J.; Van Vliet, J. P. M.; Blasse, G. *Phys. Status Solidi B* **1988**, *149*, 391–401.
(17) Endo, T.; Masuda, T.; Takizawa, H.; Shimada, M. *J. Mater. Sci. Lett.* **1992**, *11*, 1330–1332.
(18) Toda, K.; Kameo, Y.; Ohta, M.; Sato, M. *J. Alloys Compd.* **1995**, *218*, 228–232.
(19) Ida, S.; Ogata, C.; Eguchi, M.; Youngblood, W. J.; Mallouk, M. T.; Matsumoto, Y. *J. Am. Chem. Soc.* **2008**, *130*, 7052–7059.
(20) Kudo, A.; Miseki, Y. *Chem. Soc. Rev.* **2009**, *38*, 253–278.
(21) Schaak, R. E.; Afzal, D.; Schottenfeld, J. A.; Mallouk, T. E. *Chem. Mater.* **2002**, *14*, 442–448.
(22) *Measuring Quantum Yields of Powder Samples*; Hitachi High Technologies America, Inc., 2010; http://www.hitachi-hta.com/sites/default/files/appnotes/20100525-Hitachi%20QY%20Measurements-sec.pdf.
(23) Kim, J.-S.; Yang, S. C.; Bae, B.-S. *Chem. Mater.* **2010**, *22*, 3549–3555.
(24) Fujihara, S.; Tokumo, K. *Chem. Mater.* **2005**, *17*, 5587–5593.
(25) Yoo, H. S.; Im, W. B.; Kim, S. W.; Kwon, B. H.; Jeon, D. Y. *J. Lumin.* **2010**, *130*, 153–156.
(26) Kodaira, C. A.; Brito, H. F.; Felinto, M. C. F. C. *J. Solid State Chem.* **2003**, *171*, 401–407.
(27) Berdowski, P. A. M.; Blasse, G. *J. Lumin.* **1984**, *29*, 243–260.
(28) Lee, G.-H.; Kim, T.-H.; Yoon, C.; Kang, S. *J. Lumin.* **2008**, *128*, 1922–1926.
(29) Wang, H.; Yu, M.; Lin, C. K.; Lin, J. *J. Colloid Interface Sci.* **2006**, *300*, 176–182.
(30) Wells, J.-P. R.; Jones, G. D.; Reeves, R. J. *J. Lumin.* **1997**, *72−74*, 977–979.
(31) Biju, P. R.; Jose, G.; Thomas, V.; Nampoori, V. P. N.; Unnikrishnan, N. V. *Opt. Mater.* **2004**, *24*, 671–677.
(32) Lei, F.; Yan, B. *J. Solid State Chem.* **2008**, *181*, 855–862.
(33) Carlos, L. D.; Messaddeq, Y.; Brito, H. F.; Sa Ferreira, R. A.; de Zea Bermudez, V.; Ribeiro, S. J. L. *Adv. Mater.* **2002**, *12*, 594–598.
(34) Li, Y.-C.; Changa, Y.-H.; Lin, Y.-F.; Chang, Y.-S.; Lin, Y.-J. *J. Alloys Compd.* **2007**, *439*, 367–375.
(35) Xie, R.-J.; Hirosaki, N.; Kimura, N.; Sakuma, K.; Mitomo, M. *Appl. Phys. Lett.* **2007**, *90*, 191101.
(36) Jüstel, T.; Nikol, H.; Ronda, C. *Angew. Chem., Int. Ed.* **1998**, *37*, 3084–3103.
(37) Berry, M. T.; May, P. S.; Xu, H. *J. Phys. Chem.* **1996**, *100*, 9216–9222.

(38) Byeon, S.-H.; Lee, S.-O.; Kim, H. *J. Solid State Chem.* **1997**, *130*, 110–116.
(39) van Dijk, J. M. F.; Schuurmans, M. F. H. *J. Chem. Phys.* **1983**, *78*, 5317–5323.
(40) Kwon, K. H.; Im, W. B.; Jang, H. S.; Yoo, H. S.; Jeon, D. Y. *Inorg. Chem.* **2009**, *48*, 11525–11532.